

## Acicular Metallic Particles Obtained from Al-Doped Goethite Precursors

Nuria O. Nuñez,<sup>†</sup> Raul Pozas,<sup>‡</sup> M. Puerto Morales,<sup>\*,†</sup> Pedro Tartaj,<sup>†</sup>  
 Pierre Bonville,<sup>§</sup> Agustín R. González-Elipe,<sup>‡</sup> Alfonso Caballero,<sup>‡</sup>  
 Manuel Ocaña,<sup>‡</sup> and Carlos J. Serna<sup>†</sup>

*Instituto de Ciencia de Materiales de Madrid (CSIC), Cantoblanco, 28049 Madrid, Spain,  
 Instituto de Ciencia de Materiales de Sevilla (CSIC-UNSE), Americo Vespucio s/n,  
 Isla de La Cartuja, 41092 Sevilla, Spain, and CEA, CE Saclay, Service of Physique de l'État  
 Condensé, 91191 Gif-sur-Yvette, France*

*Received October 8, 2002. Revised Manuscript Received December 17, 2002*

Acicular metallic particles of different sizes were obtained by thermal treatment under a hydrogen flow of undoped and Al-doped goethite precursors. The acicular goethite particles were synthesized by the controlled oxidation–precipitation of iron (II) sulfate and aluminum nitrate solutions by addition of a base. Microstructural studies showed that the Al-doped goethite precursors consist of acicular particles with the aluminum mainly concentrated at the particle outer layers even though it was initially added during the synthesis. The mechanism for this rather atypical enrichment of aluminum can be explained in terms of the different stability of an Al-carbonate green rust phase formed during the goethite synthesis. Moreover, it was observed that the aluminum enrichment on the goethite particle surface is later enhanced during the reduction to iron. A detailed characterization of the final metal particles was carried out to correlate their chemical and magnetic properties with the structural properties of the goethite precursors. In this way, we have confirmed that the presence of aluminum is essential to preserve the acicular morphology in the metallic particles and thus, to obtain materials with good magnetic properties.

### Introduction

Nowadays, metal tapes have a widely expanded application area, including video and data information applications.<sup>1,2</sup> They essentially consist of Fe–Co acicular metallic particles (MP) doped with a minor amount of elements that confer stability to the particles against sintering and corrosion. The manufacturing process for these MP involves the use of high temperatures to first dehydrate the acicular iron oxyhydroxide precursors and finally to reduce the as-formed iron oxide particles to metallic iron. The thermal treatment can promote interparticle sintering and therefore the loss of the acicular shape. In this way, the addition of anti-sintering agents such as Al, B, Si, P, Sn, either doped or adsorbed, helps to preserve the acicular morphology of the MP.<sup>2</sup> Moreover, some of these elements increase the corrosion resistance of the particles. Therefore, to obtain fine MP with high coercivity (mainly determined by shape anisotropy) stable against oxidation, it is necessary to avoid both the sintering and the corrosion phenomena.<sup>3,4</sup>

Al-doped goethite particles have been pointed out recently as the ideal precursor for the most advanced metallic particulate recording media, although the method of synthesis and the role of this element have not been clarified.<sup>5</sup> The advantage of doping is that the Al is added during the goethite synthesis, avoiding subsequent coating of the particles.

Al<sup>3+</sup> as a commonly occurring foreign element in natural goethites has been widely investigated.<sup>6–8</sup> However, to our knowledge no detailed study has yet been made on the influence of this element in the crystallochemical and magnetic properties of the MP obtained after reduction of the goethite precursors. It is commonly accepted that Al<sup>3+</sup> is incorporated within the goethite structure up to a limit of ~30 mol %. For Al substitution lower than 10 mol %, the shape of the goethite particles has been observed to vary slightly, however, the structural defects were reduced due to a slower crystallization rate,<sup>6</sup> suggesting that the aluminum is homogeneously distributed in the goethite particles. If this particular aluminum distribution remains invariant during the transformation to metal iron, it is difficult to understand the role of this element in preserving the acicular shape of the particles and,

\* To whom correspondence should be addressed. Tel: 34-91-3348995. Fax: 34-91-3720623. E-mail: Puerto@icmm.csic.es.

<sup>†</sup> Instituto de Ciencia de Materiales de Madrid.

<sup>‡</sup> Instituto de Ciencia de Materiales de Sevilla.

<sup>§</sup> CEA.

(1) O'Grady, K.; Laidler, H. J. *Magn. Magn. Mater.* **1999**, *200*, 616.

(2) Sharrock, M. P. *IEEE Trans. Magn.* **2000**, *36*, 2420.

(3) Sugita, N.; Maekawa, M.; Ohta, Y.; Okinaka, K.; Nagai, N. *IEEE Trans. Magn.* **1995**, *31*, 2854.

(4) Onodera, S.; Kondo, H.; Kawana, T. *MRS Bull.* **1996**, Sept., 36.

(5) Hisano, S.; Saito, K. *J. Magn. Magn. Mater.* **1998**, *190*, 371.

(6) Taylor, R. M.; Schwertmann, U. *Clays Clay Miner.* **1978**, *26*, 373.

(7) Schwertmann, U.; Fitzpatrick, R. W.; Taylor, R. M.; Lewis, D. G. *Clays Clay Miner.* **1979**, *27*, 105.

(8) Bibak, A.; Gerth, J.; Borggaard, O. K. *Clays Clay Miner.* **1995**, *43*, 141.

therefore, the enhancement of their magnetic properties.

The aim of this work is to investigate the structural properties of Al-substituted goethites in an attempt to correlate the structural modifications of the precursors with the chemical and magnetic properties of the resulting metallic particles. For this purpose, Al-goethite particles with different particle sizes have been prepared by the oxidation–precipitation of Fe (II) sulfate and Al nitrate solutions by addition of a base in one or two steps, following the methods described in refs 9 and 10.<sup>9,10</sup> In the one-step method, aluminum ions can be incorporated from the beginning of the goethite particle formation. In the two-step method, the aluminum is added to the system during the second step, i.e., when some primary goethite particles are already formed. The particles so-generated have been characterized in terms of morphology, and chemical and phase composition, with special attention to determining the location of the aluminum in the particles. Finally, the magnetic properties of the MP obtained by reduction of the goethite precursors have been measured and related to their microstructure.

## Experimental Section

**Sample Preparation.** Analytical grade reagents ferrous sulfate,  $\text{Fe}(\text{SO}_4) \cdot 5\text{H}_2\text{O}$  (Fluka), aluminum nitrate,  $\text{Al}(\text{NO}_3)_3 \cdot 9\text{H}_2\text{O}$  (Aldrich), sodium carbonate,  $\text{Na}_2\text{CO}_3$  (Carlo Erba), sodium hydroxide,  $\text{NaOH}$  (Aldrich), and doubly distilled water previously deaired with  $\text{N}_2$  were used in all experiments.

Uniform Al-goethite particles were obtained by oxidation–precipitation of  $\text{FeSO}_4$  and  $\text{Al}(\text{NO}_3)_3$  solutions in one (I) or two steps (II) following the methods described earlier.<sup>9,10</sup> The molar percentage of aluminum with respect to the total cationic content used in the reactions was about 5%, which was found to be the maximum allowed in these systems to avoid both secondary phases and the destruction of the particle morphology.

When the oxidation was carried out in one step, 0.075 M Fe (II) and  $3.75 \times 10^{-3}$  M Al (III) solutions were precipitated by the addition of sodium carbonate (1.5  $\text{CO}_3^{2-}/\text{Fe}^{2+}$  molar ratio) while bubbling  $\text{N}_2$ . Immediately after, the  $\text{N}_2$  gas was replaced with air (2 L  $\text{min}^{-1}$  flow rate) and the resulting dispersion was oxidized at 40 °C during 3 h.<sup>9</sup> Samples synthesized in the absence and in the presence of aluminum by this method are named as  $\text{G}^{\text{I}}$  and  $\text{G}_{\text{Al}}^{\text{I}}$ .

When the oxidation was carried out in two steps, first, sodium hydroxide (0.35 OH/Fe equivalent ratio) was added to a 0.1 M  $\text{FeSO}_4$  solution kept at 40 °C under  $\text{N}_2$ . Immediately after, the  $\text{N}_2$  gas was replaced with air (5 L  $\text{min}^{-1}$  flow rate) until a constant pH was reached ( $\approx 3.5$ ).<sup>10</sup> Then, an appropriate amount of sodium carbonate was added to raise the pH (1.5  $\text{CO}_3^{2-}/\text{Fe}$  equivalents) and the oxidation was prolonged 4 h more at the same temperature. In this case, the aluminum ( $5 \times 10^{-3}$  M) was introduced in the second oxidation stage, i.e., together with the sodium carbonate (because it was observed that when introduced in the first stage, the morphology of the final particles was completely altered). Samples synthesized in the absence and in the presence of aluminum by this method are named as  $\text{G}^{\text{II}}$  and  $\text{G}_{\text{Al}}^{\text{II}}$ . Finally, once the reaction was completed, all the samples were cooled, centrifuged, washed several times with doubly distilled water, and collected by filtration and dried at 50 °C before analyses. Changes in the pH of the solution during synthesis were recorded using a digital pH meter (Crison GLP21).

To obtain the MP, the Al-goethite samples ( $\sim 50$  mg) were first dehydrated at temperatures between 300 and 400 °C in air during 4 h and then reduced at temperatures between 325 and 450 °C during 4 h more in a hydrogen stream of 40 L  $\text{h}^{-1}$ , 99.9999%  $\text{H}_2$ . Samples were then cooled and passivated with alcohol vapors (generated by bubbling  $\text{N}_2$  gas through an 99.8% ethanol solution) during 1 h and named as  $\text{Fe}^{\text{I}}$ ,  $\text{Fe}_{\text{Al}}^{\text{I}}$ ,  $\text{Fe}^{\text{II}}$ , and  $\text{Fe}_{\text{Al}}^{\text{II}}$ . Dehydration and reduction temperatures were optimized in each case to achieve a decrease in the internal porosity of the particles and try to preserve the acicular morphology of the MP.

**Characterization Techniques.** Phase identification was carried out by X-ray diffraction (XRD) in a Philips PW1130 using Cu K $\alpha$  radiation. A rough estimation of the crystallite size was determined from the full width at half-maximum of the reflection (110) of  $\alpha$ -Fe by using the Scherrer equation.<sup>11</sup> Cell parameters of samples were determined by a least-squares fit of the XRD data using silicon as internal reference standard. To determine the position of the diffraction peaks, single-peak fittings using a pseudo-Voigt profile were carried out. The infrared spectra of the powders diluted in KBr were recorded in a Nicolet 510 FT-IR spectrometer. Differential thermal and thermogravimetric analyses (DTA and TGA, respectively) (Seiko, EXSTAR 6000) were carried out in air at a heating rate of 10 °C  $\text{min}^{-1}$ .

The particle size and shape of samples were examined by transmission electron microscopy (TEM, Philips 300 microscope). The mean size (length (L) and width (W)) and the standard deviation (SD) associated with these two parameters were evaluated from the electron micrographs by counting approximately 100 particles. From these data, the degree of polydispersity, defined as  $\text{SD}/\text{mean size}$ ,<sup>12</sup> was evaluated. The mean and the SD values associated with the axial ratio (L/W) were evaluated from the L/W ratios obtained for each particle.

The aluminum content in the goethite samples was determined by plasma emission (ICP, Perkin-Elmer 5500). For this analysis, a 100-mg sample of powder was first dissolved with concentrated HCl and then diluted with doubly distilled water. Chemical analyses at particle level were carried out with an energy-dispersive spectrometry analyzer (QX2000, Oxford Link) integrated in the TEM. The variation of the aluminum concentration at the particle surface during the transformation from goethite to hematite, and finally to iron, was analyzed from the XPS spectra, recorded in a VG Escalab 220 using the Mg K $\alpha$  excitation source. Calibration of the binding energy scale of the spectra was done at the C1s peak of the surface carbon contamination taken at 284.6 eV. Atomic percentages of the elements were calculated from the peaks areas after background subtraction (Shirley background). The areas were referred to the sensitivity factors of the elements as supplied by the instrument manufacturers.

Temperature-programmed reduction (TPR) experiments were performed in a conventional apparatus connected to a computer for data storing and processing, using a thermal conductivity detector (TCD) calibrated with different amounts of CuO, as previously described.<sup>13</sup> The reactive gas (5%  $\text{H}_2$  in Ar, flow rate 50  $\text{cm}^3 \text{min}^{-1}$ ) was passed through 5 mg of sample, which was heated to 600 °C at a constant heating rate of 5 °C  $\text{min}^{-1}$ .

<sup>57</sup>Fe Mössbauer absorption spectroscopy was used to characterize the final iron particles. The spectra were recorded with a maximum velocity of 10 mm  $\text{s}^{-1}$  at room temperature and 4.2 K with a <sup>57</sup>Co:Rh source. By fitting the spectra at 4.2 K, the percentage of iron oxide in the final iron particles was determined. For one sample, the spectrum was recorded at 4.2 K with a magnetic field of 7 T applied parallel to the gamma ray direction. Magnetic characterization of the samples was carried out in a vibrating sample magnetometer (MLVSM9 MagLab 9 T, Oxford Instrument). Magnetization curves were

(9) Pozas, R.; Ocaña, M.; Morales, M. P.; Serna, C. J. *J. Colloid Interface Sci.* **2002**, *254*, 87.

(10) Nuñez, N. O.; Morales, M. P.; Tartaj, P.; Serna, C. J. *J. Mater. Chem.* **2000**, *10*, 2561.

(11) Azároff, L. V. *Elements of X-ray Crystallography*; McGraw-Hill: New York, 1968; p 549.

(12) Hunter, R. *Foundations of Colloid Science*; Clarendon Press: Oxford, UK, 1987; p127.

(13) Malet, P.; Munuera, G.; Caballero, A. *J. Catal.* **1989**, *115*, 567.

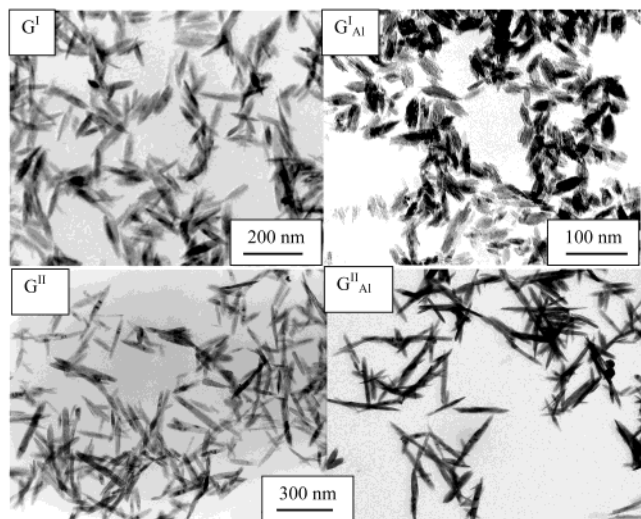


**Figure 1.** Goethite particles synthesized in the absence ( $G^I$  and  $G^{II}$ ) and the presence of aluminum ( $G^I_{Al}$  and  $G^{II}_{Al}$ ).

recorded at room temperature by first saturating the sample in a field of 3 T; then, the saturation magnetization ( $M_s$ ), the squareness ( $M_r/M_s$ , where  $M_r$  is the remanent magnetization), and the coercive field ( $H_c$ ) were determined for each sample. The  $M_s$  values were evaluated by extrapolating to infinite field the experimental results obtained in the high field range where the magnetization linearly increases with  $1/H$ .

## Results and Discussion

**Al-Substituted Goethite Particles.** Uniform goethite particles of 100 (sample  $G^I$ ) and 240 nm (sample  $G^{II}$ ) in length were obtained by oxidation of an iron (II) salt in the presence of carbonates (Figure 1), following the methods described in refs 9 and 10.<sup>9,10</sup> The presence of carbonates strongly buffered the system by keeping the pH around 10 during the growth processes, which results in rather homogeneous solids with a degree of polydispersity smaller than 25% in length for both samples.

The addition of Al during the synthesis in a percentage of 5 mol % under the conditions described in the Experimental Section also leads to single phase goethite particles with an aluminum content (determined by ICP) equal to that initially added. Chemical analyses carried out on single particles by EDX also showed a composition similar to that of the overall solid, which indicates chemical homogeneity at particle level. However, as previously observed by other authors,<sup>6–8</sup> the presence of Al affected the degree of acicularity of the particles and also the crystallinity. Thus, Al-doped goethite particles were shorter (62 and 210 nm in length for samples  $G^I_{Al}$  and  $G^{II}_{Al}$ , respectively) than those undoped, while the particle width was almost constant giving rise to a reduction in the axial ratio (Table 1, Figure 1). Additionally, the presence of aluminum drives an increase in the particle size distribution (an increase in the polydispersity degree up to 45% in the long dimension is observed for the  $G^I_{Al}$ ). Isomorphous substitution of Al for  $Fe^{3+}$  in the octahedra of the goethite structure has been pointed out as being responsible for these morphological changes.<sup>6</sup> The decrease in the unit-cell parameters,  $b$  and  $c$ , relative to those of pure goethite, was in agreement with the substitution of  $Fe^{3+}$  by the smaller  $Al^{3+}$  ion (Table 2). In contrast, the  $a$

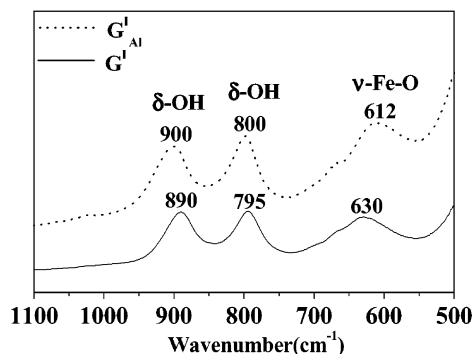


**Figure 2.** Infrared spectra for the goethite particles prepared by method I.

**Table 1. Particle Length ( $L$ ), Width ( $W$ ), and Axial Ratio ( $L/W$ ), and Al Content for the Synthesized Goethite Samples (Standard Deviations Are Included between Parentheses)**

sample	particle size (TEM)			(Al/Al+Fe) molar %	
	$L$ (nm)	$W$ (nm)	$L/W$	ICP	XPS
$G^I$	103 (25)	21 (27)	5 (2)	0	0
$G^I_{Al}$	62 (28)	23 (33)	3 (1)	5	17
$G^{II}$	240 (60)	30 (7)	8 (3)	0	0
$G^{II}_{Al}$	210 (70)	30 (8)	7 (3)	5	19

**Table 2. Unit Cell Parameters of the Goethite Samples Determined from the XRD Data**

sample	$a$ (Å)	$b$ (Å)	$c$ (Å)
$G^I$	4.622 (4)	9.956 (4)	3.028 (1)
$G^I_{Al}$	4.616 (1)	9.935 (2)	3.018 (1)
$G^{II}$	4.622 (2)	9.955 (2)	3.027 (1)
$G^{II}_{Al}$	4.621 (2)	9.943 (3)	3.017 (1)

dimension in goethite has been reported to be very sensitive to structural defects,<sup>8,14</sup> which could explain its apparently random variation. Alternatively, this variation of the cell parameters could be indicative, as previously suggested by Hazemann et al.,<sup>15,16</sup> of the presence of Al clusters within the goethite structure as a consequence of nonequilibrium crystallization processes.

An improvement in the crystallinity of the particles with Al doping was also detected in the infrared spectra of samples  $G^I$  and  $G^I_{Al}$ , according to previous works.<sup>17</sup> The spectra showed a decrease of the OH stretching frequency (data not shown) with a corresponding increase in the splitting between the two OH bending vibrations (Figure 2).

XPS spectra were registered to establish the location of the aluminum in the goethite particles. The percentages of aluminum in the particle surface determined by this technique for both samples I and II (Table 1), were much higher (around 20 mol %) than the amount added during the synthesis (~5%). This means that, within each particle, the aluminum is concentrated mainly in the outer layers independently of whether it was added at the beginning ( $G^I_{Al}$ ) or in the middle ( $G^{II}_{Al}$ ) of the synthesis process. These data would explain the increase of the thermal stability of the goethites prepared

(14) Schulze, D. G. *Clays Clay Miner.* **1984**, 32, 36.

(15) Hazemann, J. L.; Berar, J. F.; Manceau, A. *Mater. Sci. Forum* **1991**, 79–82, 821.

(16) Hazemann, J. L.; Manceau, A.; Saintavit, Ph.; Malgrange, C. *Phys. Chem. Miner.* **1992**, 19, 25.

(17) Schulze, D. G.; Schweertmann, U. *Clay Miner.* **1984**, 19, 521.



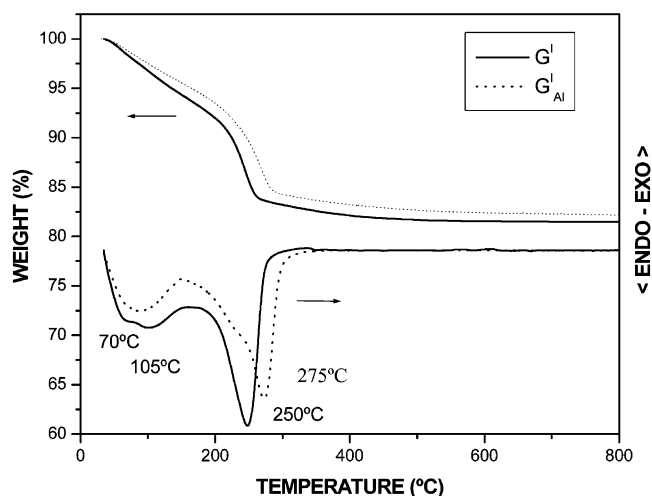


**Figure 3.** Thermogravimetric analysis of the goethite particles prepared by method I.

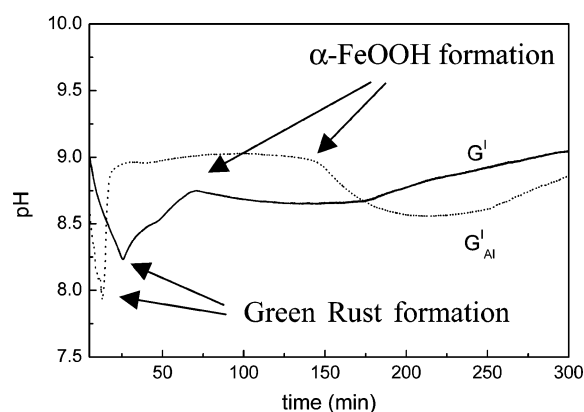


**Figure 4.** Variation of the pH during the synthesis processes of goethites following method I (the beginning of green rust and goethite formation are depicted).

in the presence of aluminum with respect to the Al-free goethites as it is observed in the TG and DTA curves for samples  $G^I$  and  $G^I_{Al}$  (Figure 3). Thus, a strong endothermic peak is observed at 250 °C and 275 °C for samples  $G^I$  and  $G^I_{Al}$ , respectively, due to the dehydroxylation and concurrent conversion of goethite to hematite. The higher temperature of dehydroxylation of sample  $G^I_{Al}$  despite having a smaller particle size, which was also observed for samples  $G^{II}$  and  $G^{II}_{Al}$ , can be attributed to the enrichment of Al on the particle surface and also to the improvement in the particle crystallinity of the Al-goethite samples.<sup>18</sup>

**Al Enrichment on Particle Surface.** As mentioned above, the Al ions in our particles are mainly concentrated in the surface, unlike Al-goethites synthesized from Fe (III) systems where the Al seems to be evenly distributed within the particles.<sup>8</sup> To understand this peculiar distribution of the aluminum, in particular for sample  $G^I_{Al}$  where aluminum was present from the beginning of the synthesis, the variation of the pH during the goethite formation in the absence and the presence of  $Al^{3+}$  was recorded (Figure 4). Because the pH changes are more prominent as increasing the iron concentration, we present only the result obtained for

a highly concentrated  $FeSO_4$  solution (0.6 M). The oxidation of the Fe (II) salt in the presence of carbonate showed an initial decrease in pH followed by a sharp increase, associated with the formation of an intermediate phase consisting mainly of a carbonate green rust and the hydrolysis of carbonates, respectively.<sup>9</sup> It is clear from Figure 4 that in the presence of  $Al^{3+}$  ions, the formation of the green rust takes place at a shorter reaction time, probably due to the reduction in the pH of the initial solution from 9 to 8.5 (associated with the strong acidic character of the  $Al^{3+}$ ). After 75 min, the pH remains almost constant for sample  $G^I$  and only at the end of the reaction is a slight increase observed. These pH variations have been associated with the green-rust decomposition producing  $\alpha$ -FeOOH and the hydrolysis of carbonate.<sup>9</sup> For sample  $G^I_{Al}$  the behavior is slightly different, detecting the beginning of the  $\alpha$ -FeOOH formation only after  $\sim 150$  min of oxidation. Thus, the presence of aluminum during the precipitation of goethite particles not only accelerates the formation of the green rust, which acts as a reservoir of iron during the goethite growth, but also retards its dissolution. Therefore, the Al-substituted green-rust appears to be much more resistant to oxidation than the Al-free intermediate. This result is in agreement with previous works about the effect of aluminum retarding the oxidation by slowing down the dissolution rate of the intermediate phase, and it may justify the influence of aluminum on the morphology and crystal order of the goethite particles.<sup>6</sup> Thus, the same effect is observed in Fe (III) systems where aluminum stabilizes ferrihydrite by slowing down its dissolution, favoring the formation of hematite.<sup>7</sup> Similar effects were also observed for goethite synthesized from Fe (II) systems in the presence of Co and Mn which are also incorporated by substitution in the goethite structure.<sup>19</sup> The fact that Al-green-rust will be the last to be dissolved to form the goethite particles explains the higher concentration of aluminum in the outer layers of the goethite particles, despite adding the Fe (II) and Al (III) ions together at the beginning of the reaction.

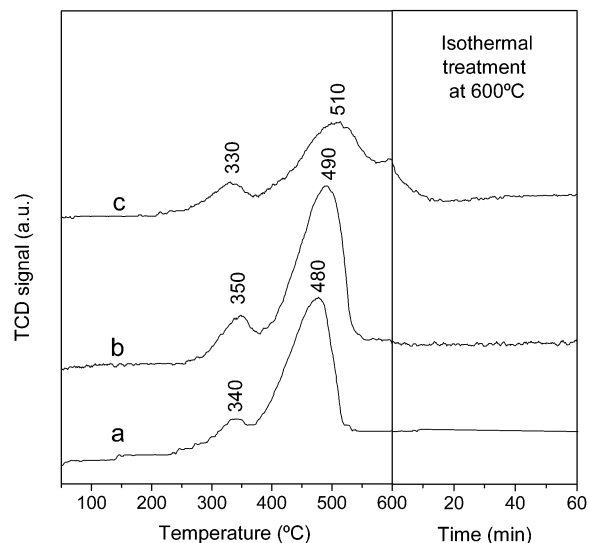
**Iron Metallic Particles.** The goethite particles were transformed to metallic iron in two steps, aiming to reduce internal porosity and avoid further alterations of the particle morphology.<sup>5</sup> First, the goethite particles were transformed to hematite by heating to a temperature high enough to eliminate the maximum number of defects, such as hydroxyl groups, inside the particle while retaining the acicular shape. This temperature was 300 °C for samples labeled as I and 400 °C for samples labeled as II. The so-obtained hematite was then reduced to metal iron, for which the reduction temperature was also optimized to minimize the possible particle sintering during this treatment. For this purpose, temperature programmed reduction (TPR) experiments were carried out. The TPR profiles of the undoped goethite samples (Figure 5a and b) clearly showed that the reduction process took place under the nonisothermal conditions, from 250 to 550 °C in two well-resolved reduction steps. The hydrogen uptakes obtained by numerical integration of the peaks areas indicated that the first step ( $\sim 350$  °C) was due to the

(18) Jónás, K.; Solymár, K. *Acta Chim. Acad. Scientiarum Hungaricae* **1970**, 6, 383.

(19) Detournay, J.; Ghodsi, M.; Derie, R. Z. *Anorg. Allg. Chem.* **1975**, 412, 184.

**Table 3. Reduction Temperature, Particle Length (*L*), Width (*W*), and Axial Ratio (*L/W*), Al and Oxide Content, and Magnetic Properties ( $M_s$  = Saturation Magnetization,  $H_c$  = Coercivity,  $M_r$  = Remanent Magnetization, and  $M_r/M_s$  = Squareness) of the Metallic Particles Obtained from the Goethite Samples Described in Table 1**

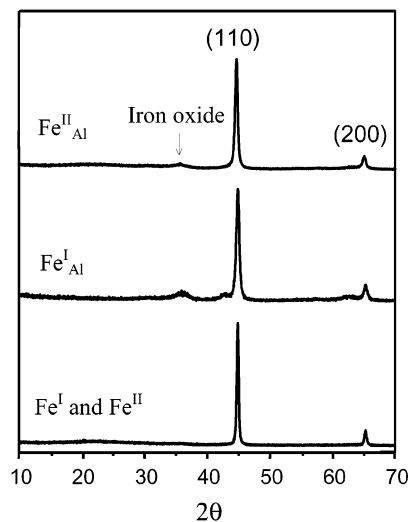
sample	reduction temp. (°C)	particle size (nm)			$M_s$ (emu/g)	$H_c$ (Oe)	$M_r/M_s$	crystal size (nm)	(Al/Al+Fe) <sub>XPS</sub> molar %	Mössbauer oxide (%)
		<i>L</i>	<i>W</i>	<i>L/W</i>						
Fe <sup>I</sup>	325	~50 nm			180	650	0.23	47	0	23
Fe <sup>I</sup> <sub>Al</sub>	400	40 (10)	18 (4)	2 (1)	128	920	0.5	24	36	44
Fe <sup>II</sup>	400	~150 nm			181	390	0.25	120	0	22
Fe <sup>II</sup> <sub>Al</sub>	450	150 (30)	21 (5)	7 (2)	137	1190	0.5	23	47	33

**Figure 5.** TPR profiles for sample  $G^I$  heated at 300 °C (a), sample  $G^{II}$  heated at 400 °C (b), and sample  $G_{Al}^I$  heated at 300 °C (c).

transformation of hematite to magnetite ( $Fe_3O_4$ ), whereas the second one (~500 °C) was due to the magnetite-metal iron reduction. It should be noted that the positions of these two maxima were slightly higher for the hematite particles obtained from sample  $G^{II}$  (350 and 490 °C) than for those from sample  $G^I$  (340 and 480 °C), which could be related to the larger particle size of the former (Table 1). Finally, the TPR profiles also suggested that the presence of Al cations in the hematite precursors (Figure 5c) retards the reduction process. In fact, an isothermal treatment at 600 °C was further required in this case to complete the reduction reaction (Figure 5). It has been reported that the reduction rate to iron is mostly controlled by the removal of water.<sup>20</sup> Therefore, it seems that the presence of Al ions at the particle surface hampers the transport of the water, needing higher reduction temperatures.

In view of these results, the hematite samples were reduced under the isothermal conditions described in the Experimental Section (using 99.9999%  $H_2$ ), at increasing temperatures starting from 300 °C. The minimum temperature required to obtain pure metallic particles was, as expected, higher for the Al-doped sample with the larger particle size (Table 3).

X-ray diffraction patterns for all the reduced samples are shown in Figure 6. Samples  $Fe^I$  and  $Fe^{II}$  display a similar pattern with only diffraction peaks due to  $\alpha$ -Fe. On the other hand, the samples containing Al show, in addition to the main diffraction peaks due to  $\alpha$ -Fe, a broad peak around 35° (2 $\theta$ ), which could be due to the

**Figure 6.** X-ray diffraction patterns for samples  $Fe^I$  and  $Fe^{II}$  (only one pattern is shown because both samples have similar ones) and samples  $Fe_{Al}^I$  and  $Fe_{Al}^{II}$ .

presence of small crystallites of an iron oxide with a spinel structure. This oxide could be formed during the passivation process carried out to stabilize the particles. The highest intensity for this peak is detected for sample  $Fe_{Al}^I$  suggesting the existence of a higher proportion of oxide, according to its smaller particle size.

Metallic particles obtained from thermal reduction of the goethite samples show very different morphological characteristics (Table 3 and Figure 7). In the absence of aluminum (samples  $Fe^I$  and  $Fe^{II}$ ), the particles lost their acicular shape as a consequence of a sintering process. In accordance, a particle volume expansion instead of a contraction was observed when going from goethite to metallic iron (Tables 1 and 3, Figures 1 and 7). Crystal sizes calculated from the X-ray diffraction peaks for these two samples are very similar to the mean size calculated from TEM (47 and 120 nm), indicating the single-crystal character of the particles (Table 3).

Although the reduction temperature of the Al (III) doped hematites had to be increased with respect to that of the aluminum free hematites, the elongated morphology of the particles was preserved (Samples  $Fe_{Al}^I$  and  $Fe_{Al}^{II}$ ) (Figure 7). Iron particles obtained from goethite coated with aluminum oxide<sup>21,22</sup> or silica oxide<sup>23</sup> also retained the acicular morphology despite requiring higher temperatures of reduction. In our case, particle

(20) Van Der Giessen, A. A.; Klomp, C. J. *IEEE Trans. Magn.* **1969**, 5, 317.

(21) Kishimoto, M.; Nakazumi, T.; Otani, N.; Sueyoshi, T. *IEEE Trans. Magn.* **1991**, 27, 4645.

(22) Lin, C. H.; Chin, T. S.; Kuo, P. C.; Chen, S. C.; Shih, C. S. *Advanced Materials '93, I/A: Ceramics, Powders, Corrosion and Advanced Processing*; Mizutani, et al., Ed. *Trans. Mater. Res. Soc. Jpn.* **1994**, 14A, 45.

(23) Ishikawa, T.; Matijevic, E. *Langmuir* **1988**, 4, 26.

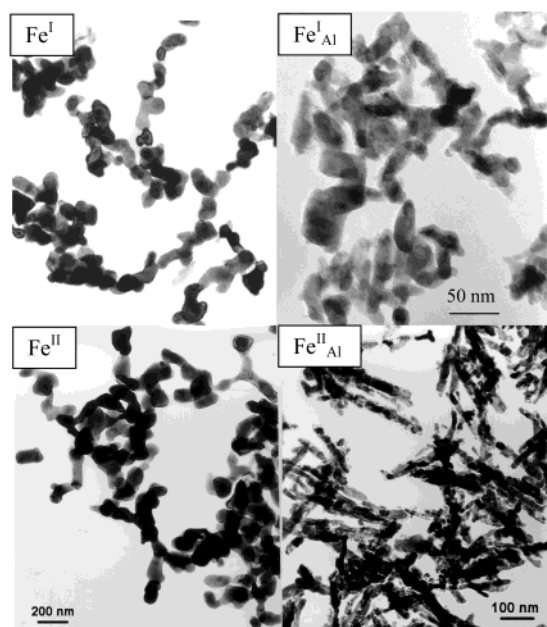


**Figure 7.** Iron metallic particles obtained by dehydration and reduction of the goethites.

length has been reduced in  $\sim 30\%$  with respect to the Al-free goethite, while the particle axial ratio was kept almost unaltered. Crystal sizes calculated for these samples by X-ray diffraction are around 23 nm, very close to the particle short dimension (Table 3). Considering that there is approximately a factor of 3 between the amount of iron in a unit volume of goethite and the same volume of iron (there are about 29 Fe atoms in  $1 \text{ nm}^3$  of goethite and about 83 Fe atoms in  $1 \text{ nm}^3$  of  $\alpha\text{-Fe}$ ), we should expect, in the absence of interparticle sintering, a shrinkage of the volume of about a factor of 3 in the samples that keep the axial ratio after reduction ( $\text{Fe}^{\text{II}}_{\text{Al}}$ ). Indeed, this is the case (Tables 1 and 3), which clearly indicates the absence of interparticle sintering.

The role of the aluminum to preserve the acicular morphology can be better understood by studying the variation of its concentration at the particle surface during the transformation from goethite to hematite, and then, to metal iron. This study was followed by XPS and the data are shown in Figure 8. The molar percentage of aluminum increases from 17–19 to 36% in the case of sample  $\text{Fe}^{\text{I}}_{\text{Al}}$  and to 47% for sample  $\text{Fe}^{\text{II}}_{\text{Al}}$ . Thus, there is a clear enrichment of the particle surface in aluminum during the reduction of both samples, which helps to enhance its antisintering effect. The XPS spectra also revealed that, as expected, the oxidation state of aluminum was not altered by the reduction process. In addition, the position of the observed  $\text{Fe}2p_{3/2}$  XPS peak (710.1 eV) was consistent with the presence of oxidized iron in the particles' outer layers, in agreement with the X-ray diffraction data (Figure 6).

The  $^{57}\text{Fe}$  Mössbauer spectra at 4.2 K for the metallic iron samples support the above results (Figure 9a). The spectra for all the samples consist of two sextets, one corresponding to metallic iron with a hyperfine field of 34 T and another with a larger hyperfine field around 50 T and relatively broad lines, characteristic of an iron oxide with a spinel structure.<sup>24</sup> Iron oxide percentages of 22–23% were obtained from the spectra for Al-free samples, but this percentage increases up to 44% for

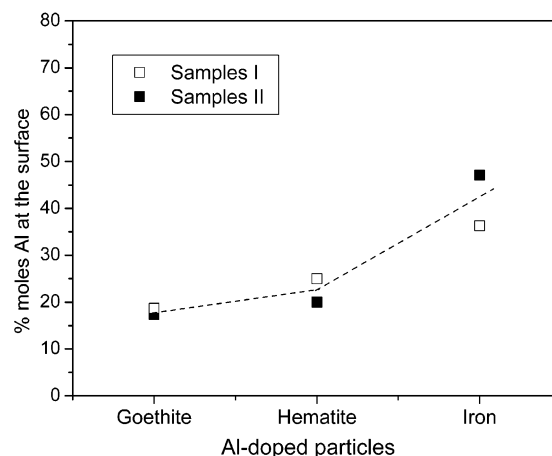


**Figure 8.** Variation of the aluminum concentration calculated from XPS during the transformation from goethite to hematite and finally to metal iron for the samples synthesized by methods I and II.

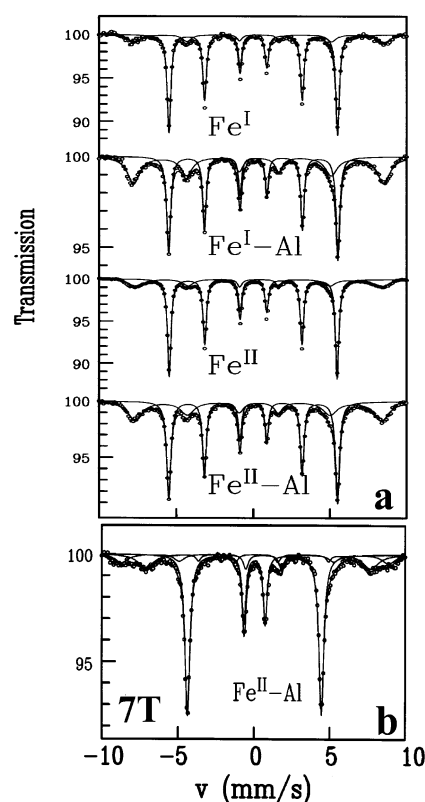


**Figure 9.** Mössbauer spectra at 4.2 K (a) for the iron metallic particles; b) for sample  $\text{Fe}^{\text{II}}_{\text{Al}}$  in the presence of an applied field of 7 T parallel to the direction of the  $\gamma$ -ray.

the sample with the smallest particle size ( $\text{Fe}^{\text{I}}_{\text{Al}}$ ). These percentages can be attributed to an oxide layer around the particle surface that is produced during the passivation process and is responsible for the stabilization of the iron metallic particle against oxidation.<sup>25</sup> In the case of samples  $\text{Fe}^{\text{I}}_{\text{Al}}$  and  $\text{Fe}^{\text{II}}_{\text{Al}}$ , taking into account the particle size obtained from TEM (Table 3) and the content in iron oxide determined by Mössbauer (44 and 33%, respectively), we can estimate an iron–aluminum

(24) Greenwood, N. N.; Gibb, T. C. *Mössbauer Spectroscopy*; Chapman and Hall: London, UK, 1971.

(25) Parker, F. T.; Spada, F. E.; Cox, T. J.; Berkowitz, A. E. *J. Appl. Phys.* **1995**, *77*, 5853.



oxide layer between 2 and 3 nm thick. At room temperature, the Mössbauer spectrum of the oxide consists of a broad unresolved line or a broad quadrupolar doublet (data not shown) confirming that the oxide occurs as small particles or as a thin surface layer.

Further confirmation about the nature of the oxide layer at the particle surface was obtained from the Mössbauer spectrum of sample  $\text{Fe}^{\text{II}}_{\text{Al}}$  recorded at 4.2 K in the presence of an applied magnetic field of 7 T (Figure 9b). The spectrum was fitted with three sextets, one assigned to the metal iron core perfectly aligned with the magnetic field (extinction of the intermediate lines), and the other two sextets assigned to a ferrimagnetic oxide similar to maghemite with two sublattices corresponding to the A and B sites of a spinel structure. The  $\text{Fe}^{3+}$  ions of the oxide are affected by spin canting (presence of intermediate lines) with important canting angles according to its location at the surface.

The magnetic parameters obtained from the hysteresis loops are shown in Table 3. As to the saturation magnetization, all the values (see Table 3) are well below that for  $\alpha\text{-Fe}$  ( $220 \text{ emu g}^{-1}$ )<sup>26</sup> due to the presence of the ferric oxide layer at the particle surface. The largest  $M_s$  values were obtained for the samples with the largest particle size and consequently lower percentage of iron oxide with respect to metal iron (Samples  $\text{Fe}^{\text{I}}$  and  $\text{Fe}^{\text{II}}$ ). By using the atomic percentages of Fe in the metal and in the oxide (assumed to be maghemite nanoparticles ( $\sim 2 \text{ nm}$ ) with a small saturation magnetization of  $\sim 10\text{--}20 \text{ emu g}^{-1}$ )<sup>27</sup> obtained from the Mössbauer spectra at 4.2 K, we can calculate the saturation magnetization of the iron core  $M_s(\text{Fe})$  which was for all samples about  $220 \text{ emu g}^{-1}$ , close to the bulk value. This result is not surprising because it has been previously reported that even in Fe nanoparticles of about 3 nm in size, the magnetic structure is similar to that of the bulk Fe.<sup>28</sup>

The protection effect of the aluminum against interparticle sintering during the reduction has a very favorable effect on the coercivity of the metallic powders (Table 3). The coercivity increases from 390 to 650 Oe for the Al-free samples to 1190 Oe for the sample where the particle morphology was well preserved and has the largest axial ratio ( $\text{Fe}^{\text{II}}_{\text{Al}}$ ). In addition, the increase in the  $M_r/M_s$  values from 0.2 to 0.5 suggests that the magnetic behavior changes from multidomain for Al-free samples to monodomain for Al-doped samples (Figure 10). Therefore, Al-doped goethite particles can be transformed to metal iron preserving the morphology because of the concentration of the aluminum in the outer layers of the particle. Besides, the antisintering effect of aluminum is more efficient when the aluminum is introduced in the final stage of the goethite formation

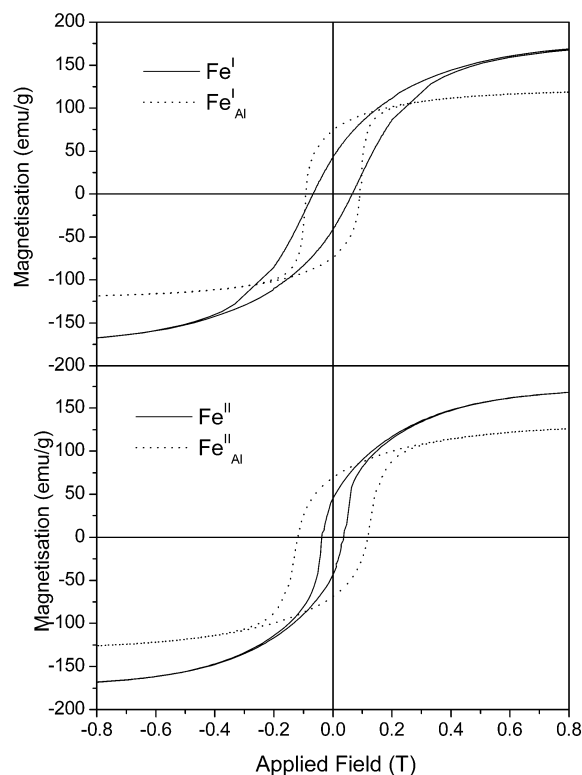


**Figure 10.** Magnetization curves at room temperature for the iron metallic particles.

rather than at the beginning of the reaction, because the morphology protection is more effective.

### Conclusions

Acicular Al-doped goethite particles of different sizes prepared by the oxidation–precipitation of iron (II) sulfate and aluminum nitrate solutions have the aluminum cations mainly concentrated in the outer layers, unlike the even distribution of aluminum observed in Al-goethites synthesized from Fe (III) systems. It has been found that this enrichment of aluminum is associated with the formation of an Al-carbonate green rust during the synthesis that is very stable against dissolution. We have also found that only the Al-doped goethites particles can be transformed to metallic iron preserving the morphology because of the enrichment of aluminum in the outer layers of the particle. Mössbauer and magnetic studies have allowed us to conclude that the metallic particles consist of an iron core with characteristics similar to those of bulk Fe surrounded by an Al-maghemite surface layer. Finally, we have determined that, as expected, the best coercivity is detected for those samples that have the largest axial ratio.

**Acknowledgment.** This work was supported by the CICYT under project PB98-0525. N.O.N. and R.P. gratefully acknowledge their fellowships from the Agencia Española de Cooperación Iberoamericana and the Spanish Ministerio de Ciencia y Tecnología, respectively.

CM021329H

(26) Cullity, B. D. *Introduction to Magnetic Materials*; Addison-Wesley: Reading, MA, 1972.

(27) Morales, M. P.; Veintemillas-Verdaguer, S.; Montero, M. I.; Serna, C. J.; Roig, A.; Casas, L.; Martínez, B.; Sadiumenge, F. *Chem. Mater.* **1999**, *11*, 3058.

(28) Bødker, F.; Mørup, S.; Linderth, S. *Phys. Rev. Lett.* **1994**, *72*, 282.